Drug Design, Development and Therapy

Dovepress
Taylor & Francis Group

Open Access Full Text Article

ORIGINAL RESEARCH

Structure-Based Virtual Screening of New Skp1 Inhibitor Chemotypes Targeting F-Box Binding Interface

Muzammal Hussain[1–3], Yongzhi Lu[1,4], Gui-Zhen Wang[5], Muqddas Tariq[1,2], Jiancun Zhang[1,2], Guang-Biao Zhou[5], Jinsong Liu[1,2,6]

[1]Center for Chemical Biology and Drug Discovery, Guangzhou Institutes of Biomedicine and Health, Chinese Academy of Sciences, Guangzhou, 510530, People's Republic of China; [2]Guangdong Provincial Key Laboratory of Biocomputing, Institute of Chemical Biology, Guangzhou Institutes of Biomedicine and Health, Chinese Academy of Sciences, Guangzhou, 510530, People's Republic of China; [3]Current Address: Department of Biochemistry and Molecular Pharmacology, New York University Grossman School of Medicine, New York, NY, 10016, USA; [4]School of Basic Medical Sciences, Guangzhou Laboratory, Guangzhou Medical University, Guangzhou, 510005, People's Republic of China; [5]State Key Laboratory of Molecular Oncology and Department of Internal Medicine, National Cancer Center/National Clinical Research Center for Cancer/Cancer Hospital, Chinese Academy of Medical Sciences and Peking Union Medical College, Beijing, People's Republic of China; [6]Pamplona Therapeutic Co. Ltd., Shenzhen, 518052, People's Republic of China

Correspondence: Jinsong Liu, Pamplona Therapeutic Co. Ltd., Shenzhen, 518052, People's Republic of China, Email jinsong.liu@pamplonatx.com; Muzammal Hussain, Department of Biochemistry and Molecular Pharmacology, New York University Grossman School of Medicine, New York, NY, 10016, USA, Email hmuzammal0404@gmail.com

Background: Skp1 is a potential pharmacological target for cancer treatment. However, the few Skp1 inhibitors reported to date have exhibited limited structural diversity and target specificity. This highlights the need for new chemical scaffolds that could potentially be developed into potent and specific Skp1 inhibitors.

Methods: We performed a large-scale, hierarchical, structure-based virtual screening (SBVS) integrated with molecular dynamics (MD) simulations against a hydrophobic and shallow P1 hotspot region within the F-box binding interface of Skp1, using a commercial compound library (~280,000 compounds). The top-ranked hits were then experimentally validated using in vitro biophysical and biochemical assays, followed by evaluation of cell viability.

Results: The SBVS campaign yielded 28 potential hits. Using a thermal stability shift assay (TSA), we confirmed that several compounds directly bind to both full-length Skp1 and its truncated variant containing only the P1 hotspot ($Skp1^{1-140}$), consistent with the SBVS strategy. Functional inhibition assessed by a fluorescence polarization (FP) assay showed that compounds #03, #05, #07, #09, #22, #24 and #28 effectively disrupted the Skp1:F-box peptide interaction in vitro. Furthermore, compounds #04, #12, #15, and #24 demonstrated low-to-moderate micromolar EC_{50} values in cell viability assays across different cancer cell lines.

Conclusion: Compounds #04, #12, and #24 represent interesting scaffolds and may serve as valuable starting points for future structure-activity relationship (SAR) studies aimed at developing a new class of selective Skp1 inhibitors.

Keywords: virtual screening, Skp1 inhibitors, molecular docking, molecular dynamics simulation, binding free energy, hydrophobic hotspot

Introduction

S phase kinase-associated protein 1 (Skp1) serves as an adapter component of Skp1-Cullin 1-F-box protein (SCF) ubiquitin ligases (Figure 1).[1,2] Aberrant SCF E3 activity, whether through abnormally active SCF ligase complexes or dysregulation of individual components such as Cullin 1,[3,4] Rbx1,[5,6] and several F-box proteins (eg. Skp2, FBXL10, β-TRCP, etc.),[7,8] may promote tumor growth and progression. Emerging data also indicate that Skp1's aberrant expression-(s) may contribute to malignant transformation and tumor development.[9–16] For instance, a previous study by Tian et al showed that Skp1 upregulation promotes YAP-mediated stemness of colorectal cancer stem cells and predicts poor prognosis in patients with colon cancer.[11] Two other studies, including our previous work,[12,13] manifested that Skp1

https://doi.org/10.2147/DDDT.S578211
Received: 31 October 2025
Accepted: 22 March 2026
Published: 30 March 2026

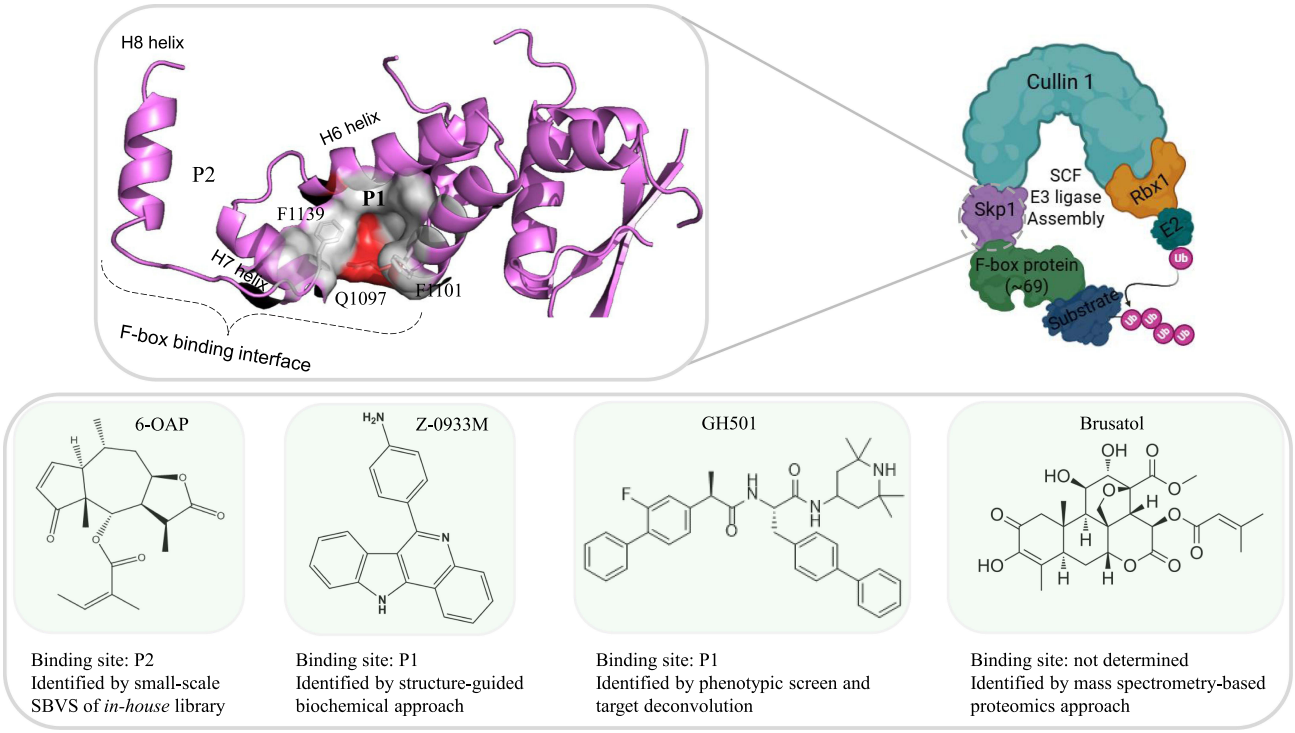

Figure 1 SCF assembly and reported Skp1 inhibitors. Each individual SCF E3 ligase is composed of four core components: Skp1, Cullin 1, Rbx1, and a member of the ~69-memebr F-box protein family.

overexpression is critical for lung cancer cell proliferation and survival and is associated with poorer patient outcomes. A more recent study by Quan et al demonstrated that Skp1 overexpression may compromise or rescue the tumor-suppressive effects of FBXO32 in glioma cells, thus implicating a tumor-promoting potential of Skp1 in glioma progression.[14] Moreover, circRNA (circGLIS3)- and lncRNA (CCDC183-AS1)-mediated upregulated expressions of Skp1 have been implicated in promoting the proliferation of bladder cancer cells and the progression of hepatocellular carcinoma, respectively.[15,16]

In recent years, there has been growing interest in developing SCF-targeting anticancer agents.[17–19] Several small-molecule inhibitors have been reported that act at different stages of SCF assembly, including: upstream (Cullin neddylation, eg. MLN4924),[20] mid-level (Skp1:F-box protein-protein interaction, eg. Skp1/Skp2 inhibitors),[12,21,22] and downstream (substrate recognition, eg. inhibitors of Skp2/p27 or Skp2/Cks1 interactions).[23,24] Because Skp1:F-box protein-protein interactions (PPIs) are a prerequisite for assembling intact and active SCF E3 ligase complexes,[2] pharmacologically disrupting these PPIs represents an attractive strategy. Unlike the selective inhibition of individual F-box proteins (eg. Skp2),[22] small-molecule targeting of Skp1:F-box PPIs offers the potential to disrupt the broader SCF E3 ligase machinery, which may be particularly advantageous in treating highly heterogeneous tumors.[12,21,25] In this context, our previous work,[12,21] along with that of others,[25,26] has demonstrated that small-molecule targeting of the F-box binding interface on Skp1 is feasible and effectively disrupts Skp1:F-box PPIs. Importantly, such interventions have shown growth-suppressive effects in tumor cells and eradicated tumor growth in preclinical xenograft models of lung and castration-resistant prostate cancers.[12,21,25,26] This highlights the potential of Skp1 as a therapeutic target for cancer treatment. Nevertheless, given the central role of Skp1 in coordinating multiple SCF complexes, broad disruption of Skp1:F-box interactions may also carry risks related to context-dependent effects in normal tissues.[2,27] Therefore, context-specific targeting will be an important consideration in the future development of Skp1-direted therapeutics.

The chemical pipeline reported thus far for targeting the F-box binding interface of Skp1 remains thin and displays little chemical diversity. As shown in Figure 1, only a few compounds, including 6-OAP,[12] Brusatol,[25] Z0933M [21], and GH501,[26] have been reported. Nevertheless, questions remain regarding target specificity and translational potential of

many of these compounds. Brusatol has long been recognized for its tumor-suppressive effects via Nrf2 targeting and disruption of associated pathways,[28] and exhibits high non-specific toxicity in animals.[29] 6-OAP, a natural compound, has low effectiveness[12] and was subsequently revealed to augment its anti-tumor effects by targeting STAT3.[30] Likewise, Z0933M, a structural analog of the anti-tuberculous compound Z0933,[31] has weak or no anti-proliferative activity against p53 deficient (null or mutant) cell lines. Hence, the discovery of new scaffolds with the potential to serve as effective drug candidates against Skp1 is imperative.

From a drug discovery perspective, none of the currently reported Skp1 inhibitors has been identified through large-scale, structure-based virtual screening (SBVS) (Figure 1). In this study, we therefore employed a molecular dynamics (MD)-integrated SBVS approach using a commercial compound library to discover new chemotypes with potential Skp1 inhibitory activity. Subsequent experiments led to the identification of new small-molecule scaffolds that could serve as the starting points for the development of next-generation Skp1 inhibitors.

Methods

Preprocessing of the Target Protein Skp1 Structure

The Skp1 structure from the crystal structure of Skp1-Skp2-Cks1 in complex with a p27 peptide (PDB: 2AST) was retrieved and used for molecular docking. The structure was preprocessed for SBVS Glide-docking using the Protein Preparation Wizard in Maestro (Schrödinger Suite, LLC, New York, NY, 2012). Hydrogen bonds were optimized, and restrained minimization was performed to relax the structure. The receptor grid was generated using the Glide Grid Generation module, with the grid box centered directly on the F-box binding interface of Skp1. An enclosing box of 20 Å covering the P1 residues was defined, while other parameters were kept at their default values.

For AutoDock Vina flexible docking (used as a subsequent cross-validation step in SBVS workflow), the protein was prepared using AutoDock Tools.[32,33] Separate PDBQT files were prepared for the rigid portion of the protein and the flexible sidechains of P1 residues. The exhaustiveness and num_modes were set to 50 and 100, respectively.

Pretreatment of Ligand Library

The SPECS database subset was downloaded from the ZINC website (http://zinc.docking.org). The structures of the compounds were prepared using LigPrep (LigPrep, version 2.5, Schrödinger, LLC, New York, NY, 2012). The preprocessing steps included protonation, desalting and addition of hydrogen atoms, followed by the generation of possible tautomeric and stereochemical states to account for structural flexibility. Subsequently, energy minimization was performed to ensure the stability and chemical plausibility of each compound. For molecular docking using AutoDock Vina, the shortlisted compounds were converted into the PDBQT format using OpenBabel, which defined torsional degrees of freedom and partial charges according to the docking requirements.

Docking and SBVS

SBVS was performed in hierarchical manner by using the Schrödinger software package (Schrödinger Suite, LLC, New York, NY, 2012). Molecular docking was performed with the Glide (Grid-based ligand docking energetics) software (Schrödinger, Mannheim, Germany), which was run from the graphical Maestro interface (Schrödinger, Mannheim, Germany). The standard precision (SP) and extra precision (XP) Glide dockings were performed as the initial enrichment steps. The poses obtained from docking calculations were ranked using an energy-based scoring function. Analyses of ligand-protein interaction(s) were performed using the graphical interfaces of Maestro (Schrödinger, Mannheim, Germany) and PyMOL version 1.8.8.2. The docked compounds were subsequently filtered using Discovery Studio 3.5 to evaluate their drug-likeness according to Lipinski's rule of five and Veber's criteria,[34] followed by ADMET (Absorption, Distribution, Metabolism, Excretion, and Toxicity) predictions to assess the key pharmacokinetic and safety parameters. The computed properties included aqueous solubility, human intestinal absorption, Caco-2 cell permeability, blood-brain barrier (BBB) penetration, plasma protein binding (PPB), cytochrome P450 2D6 (CYP2D6) inhibition, and hepatotoxicity. Compounds exhibiting good intestinal absorption (level 0), acceptable solubility (levels 2–4), high permeability (levels 2–3); reasonable BBB penetration (levels 0–1); and moderate PPB (level 1) were considered to be

favorable. In addition, molecules predicted to be non-inhibitors of CYP2D6 (level 0), non-hepatotoxic (level 0), and non-mutagenic/non-carcinogenic (level 0) were retained for further analyses. An overall ADMET score ≤3 was used as the final threshold for compound selection. Following ADMET-based filtering, the selected compounds were clustered using 2D binary molecular fingerprints in Canvas (version 1.5, Schrödinger, LLC, New York, NY, 2012) to assess their chemical diversity. A total of 300 clusters were generated, and the top-scoring representative compound from each cluster was selected for subsequent cross-validation using a different program, AutoDock Vina. Finally, compounds passing a concurrent criterion of chemical diversity, reasonable binding poses, and docking scores were subjected to MD simulations to assess the stability and dynamics of ligand-protein interactions.

MD Simulations

MD simulations were performed using the Amber 14 package and following a protocol as described previously.[35] Briefly, the initial orientations of the selected compounds from enrichment steps of SBVS were determined from the docking poses of Glide. The Amber ff14SB force field and the general Amber force field (GAFF)[36] were used for the protein and ligands, respectively. Then, complex structures were solvated using a cubic box of TIP3P water molecules,[37] which were extended at least 10 Å away from the boundary of any protein atoms. An appropriate number of Na^+ and Cl^- ions were added to neutralize the system. Each system was then subjected to energy minimization. First, water molecules, hydrogen atoms, and salt ions were subjected to 2500 steps of steepest descent minimization and 2500 steps of conjugate gradient minimization, whereas other heavy atoms were constrained with a harmonic force of 50 kcal mol^{-1} $Å^{-1}$. Next, the heavy atoms were constrained with a harmonic force of 25 kcal mol^{-1} $Å^{-1}$ and minimized with 2500 steps of steepest descent minimization and 2500 steps of conjugate gradient. The system was then heated from 0 K to 300 K and equilibrated for 500 ps. Finally, 80 ns long simulations without restriction were conducted for each ligand-protein complex at a constant pressure and temperature (T = 300 K, P = 1 atm). During MD simulations, the SHAKE method was applied to constrain the covalent bonds involving the hydrogen atom.[38] The Particle Mesh Ewald (PME) method was adopted to treat long-range electrostatic interactions. The cutoff distances for the long-range electrostatic and van der Waals interactions were set to 10 Å. Root mean square deviation (RMSD) of the Cα was calculated from the MD trajectories at 100 ps intervals. As part of SBVS strategy, the average 1000 snapshots for each system were extracted from the last 10 ns of MD trajectory at 10 ps intervals, and the relative binding free energies (ΔMM/GBSA and ΔMM/PBSA) were determined using the MM/PBSA and MM/GBSA procedures implemented in Amber 14. Compounds exhibiting stable RMSD trajectories, with fluctuations not exceeding 2 Å throughout the simulation period, were considered to be structurally stable within the binding pocket. These compounds were prioritized for procurement and subsequent in vitro experimental validation.

Compounds Source

The compounds selected from SBVS were purchased from SPECS Corp. (Netherlands) and prepared as stock solutions of 50 mM in DMSO.

Protein Expression and Purification

Skp1 protein(s) was expressed and purified by following the protocol as reported previously.[21] In brief, the pETDuet-1 vector was used to express Skp1 wild type ($Skp1^{WT}$) and Skp1 truncate ($\Delta Skp1^{1-140}$) as His6-fusion protein(s) in *Escherichia coli BL21*(DE3) cells. After overnight induction with 0.5 mM isopropyl-b-D-thiogalactopyranoside (IPTG) at 16°C, the cells were harvested by centrifugation (4,000 rpm, 20 min, and 4°C) using a Beckman Coulter Avanti J-20 XP centrifuge. The pellets were lysed in a buffer containing 50 mM Tris-HCl (pH 8.0), 500 mM NaCl, 20 mM imidazole, 7 mM β-mercaptoethanol, and 1 mM phenylmethylsulfonyl fluoride (PMSF). Protein purifications were conducted by subjecting the clarified bacterial cell lysates to a three-step purification process, including Ni-affinity chromatography, ion exchange chromatography, and size-exclusion chromatography (SEC), using Akta FPLC (GE Healthcare). The purified protein was concentrated by centrifugal ultrafiltration and stored at −80°C in small aliquots.

In vitro Compound(s) Testing Using Biophysical and Biochemical Assays

In vitro testing of shortlisted compounds was conducted using thermal stability shift assay (TSA), also known as differential scanning fluorimetry (DFS), and fluorescence polarization (FP) assay by following the protocols as described previously.[21] For TSA, protein samples at final concentration of 8 μM were mixed with 200 μM of final ligand(s) in a final volume of 10μL in a 96-well plate with 1x SYPRO Orange (Invitrogen). After 30 min incubation, the samples were heated at 0.5°C per minute, ranging from 30 to 90°C, and the fluorescence intensity was measured at the interval of 0.5°C. The shift in melting temperature (T_m) was measured as $\Delta T_m = T_m$ (ligand-protein) – (protein-only), and the resultant values were plotted using GraphPad Prism (v6.0; San Diego, CA).

For FP assay, a C-terminally fluorescently labeled F-box peptide (tracer) comprising 50 amino acids (RENFPGVSWDSLPDELLLGIFSCLCLPELLKVSGVCKRWYRLASDESLWQ-FAM) was purchased from Yuan Peptide (Shanghai, China). This tracer was designed based on the consensus sequence of the Skp2-F-box motif (PDB ID: 2AST, Chain B). The optimization of the direct binding of tracer to Skp1 and assay quality has been described previously.[21] For the initial screening of SBVS-selected compounds, competitive FP experiments were conducted at a final compound concentration of 250 μM. Briefly, reactions (20 μL final volume in quadruplicates, black Costar 384-well plate) containing 25 μM $Skp1^{WT}$, 500 nM tracer (F-box-FAM), and 250 μM of each test compound were incubated for 2 h at room temperature. The control reactions included free F-box-FAM (tracer), bound $Skp1^{WT}$-F-box-FAM, and FP buffer only (20 mM Tris-HCl pH 8.0, 150 mM NaCl, 2 mM DTT, 5% (v/v) glycerol, 0.001% (v/v) Triton X-100). FP signals were recorded on an EnVision multilabel reader at an excitation wavelength of 485nm, and emission was detected at 535nm. The resultant FP values were analyzed and plotted as bar graphs using GraphPad Prism (v6.0; San Diego, CA).

Anti-Proliferative Evaluation

The lung cancer cells (A549), hepatocellular carcinoma cells (HepG2), colorectal cancer cells (HCT116), and breast cancer cells (MCF-7) were originally obtained from ATCC and cultured under standard conditions as previously described.[12,21] Cell viability following compound(s) treatment was evaluated using the MTT assay, as reported previously.[12] Briefly, exponentially growing cells (1×10^4 in 180 μL) were seeded in 96-well microplates and allowed to adhere overnight. Subsequently, 20 μL of each compound (10× concentrated) was added to achieve the desired final concentration. After incubation with or without the test compound(s) for 44 h, 100 μg MTT reagent was added to each well and incubated for 4 h. The plates were then centrifuged, and the resulting MTT formazan crystals were dissolved in 150 μL DMSO. The plates were agitated on a microplate shaker for 5 min to ensure complete solubilization, and absorbance was measured at 570 nm using a multiplate reader.[12]

Results

SBVS Accompanied by MD Simulations Predicted 28 Potential Hits

For SBVS, the dynamic stability of the binding site of target protein is of critical importance.[39,40] Nevertheless, the F-box binding interface of Skp1 does not comprise a well-defined pocket (Figure 1). Instead, it features a shallow "P1" hotspot region adjacent to a structurally unstable C-terminal extension, designated as "P2" (H8 helix).[41] Our preliminary 200 ns MD simulations of apo Skp1 (Figure S1) revealed pronounced conformational flexibility within the P2 region, whereas the P1 hotspot exhibited relatively better structural stability. Our previous work also provided the rationale that small-molecule intervention at the P1 hotspot represents an attractive strategy to disrupt Skp1:F-box PPIs.[21] A recent study on the GH501 compound further corroborates this notion.[26] Therefore, we focused on P1 hotspot in our SBVS campaign.

As depicted in Figure 2A, a hierarchical SBVS strategy was adapted considering the time and enrichment efficiency. Approximately 280,000 molecules from the SPECS database were downloaded from the ZINC website. For the first run, the SP mode of Glide docking was used to rank the compounds. For the second run, a new drug library was generated consisting of the 10% best-evaluated structures from the first run. The screening settings were switched from SP to XP docking. The best 10% results of this run were gradually filtered by Lipinski and Veber rules,[34] and by ADMET (Absorption, Distribution, Metabolism, Excretion, and Toxicology) analysis using Discovery Studio 3.5. The remaining 1,997 compounds were clustered using Canvas (version 1.5, Schrödinger, LLC, New York, NY, 2012), and 353 compounds were then chosen for cross-validation using a different docking algorithm, AutoDock Vina.[32] Considering

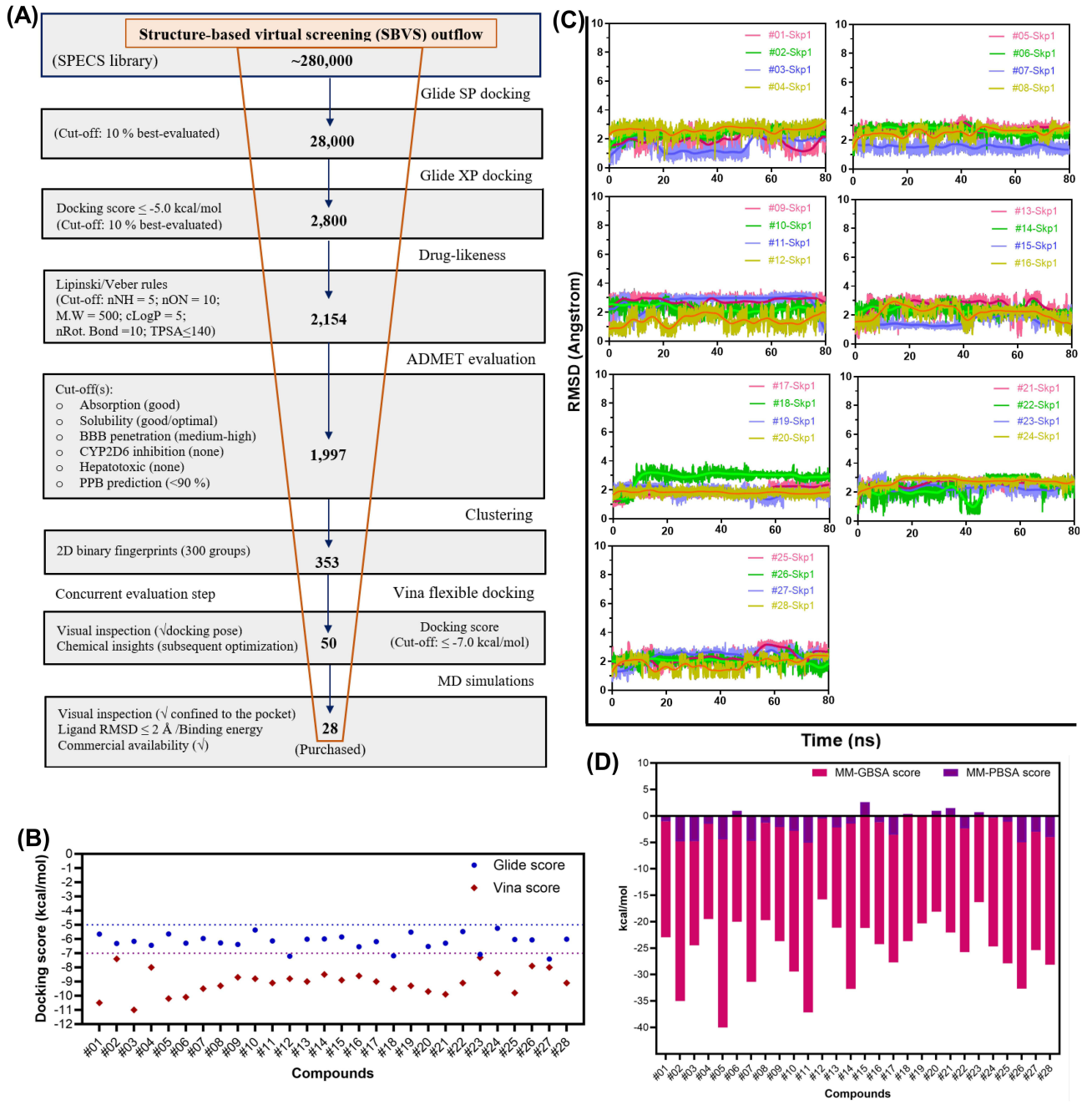

Figure 2 SBVS workflow and computational analysis. (**A**) Schematic representation of the hierarchical SBVS process. The red box highlights the compounds retained after each SBVS filtering step. (**B**) Docking score distribution of the Glide (XP) and AutoDock Vina poses for the 28 shortlisted compounds. The blue dotted horizontal line indicates the Glide cut-off docking score (−5 kcal/mol), and the red dotted line denotes the Vina cut-off score (−7 kcal/mol). # denotes the compound number. (**C**) RMSD graphs over 80 ns MD trajectories for the 28 Skp1-compound complexes. (**D**) Comparative of MM/GBSA and MM/PBSA binding free energy estimates calculated from final 10 ns of each MD trajectory.

the intrinsic structural flexibility of the F-box binding interface of Skp1, flexible docking was employed to allow for local conformational adjustments of key residues and ensure that alternative binding modes were adequately explored. From this set, 50 compounds that passed a concurrent criterion of chemical diversity, reasonable binding poses and consistent interaction profiles across both docking platforms were shortlisted and subjected to MD simulations to evaluate the stability and persistence of their binding under dynamic conditions.

The docking scores, RMSD plots, and binding free energies calculated from the snapshots extracted from the last 10 ns of MD trajectories are presented in Figure 2B–D. The chemical structures and interacting residues of each compound, as

https://doi.org/10.2147/DDDT.S578211

determined by analysis of their binding poses (Figure S2), are illustrated in Figure 3. Interaction analyses revealed that the selected compounds primarily engaged in hydrophobic contacts within the P1 region. In particular, most short-listed compounds exhibited dual stacking π-π or π-cation interactions with two phenylalanines (F1101 and F1139), along with a hydrogen bonding (H-bond) interaction with Q1097. These interaction patterns were consistent with the rationale of our previous study, which stated that the aromatic cage formed by the two phenylalanine residues constitutes an attractive hotspot for small-molecule drug discovery against Skp1.[21] The RMSD profiles of the most compounds exhibited relatively minor fluctuations and remained well-converged throughout the simulation period (Figure 2C), suggesting stable ligand-protein interactions and sustained binding within the P1 binding site. Nevertheless, a few compounds, such as #01, #03, #12, #22, #25, and #28, displayed moderate conformational flipping, although these fluctuations remained ≤ 2 Å. Visual inspection of the MD trajectories confirmed that these compounds remained bound within the binding site, and the observed fluctuations were primarily attributed to the intrinsic conformational and structural flexibility of the F-box binding interface of Skp1. Likewise, compound #18 exhibited an initial displacement during the first 5 ns of the simulations but subsequently stabilized and maintained a consistent binding pose thereafter. Overall, the shortlisted compounds showed stable and sustained interactions with the P1 region, highlighting their potential as reliable binders of Skp1.

Re-evaluating and re-scoring of the initial docking hits with MD simulations combined with MM/GBSA and MM/PBSA analyses improved the overall enrichment in the final selection stage. However, we placed greater emphasis on the visual inspection of MD trajectories and the stability of ligand-protein complexes particularly monitoring RMSD fluctuations (≤2 Å) throughout the simulations (Figure 2C). One key reason for not relying heavily on MM/PBSA or MM/GBSA re-scoring was the hydrophobic and partially flexible nature of the Skp1 binding interface. In such cases, these methods may often underestimate the entropic contribution arising from water displacement and protein conformational dynamics, leading to less accurate estimations of true binding affinities.[42,43]

Interestingly, the binding energies estimated by both the MM/GBSA and MM/PBSA methods reflect the hydrophobic character of the P1 hotspot region. Most of the shortlisted compounds exhibited binding energies around −20 kcal/mol with MM/GBSA, whereas MM/PBSA produced relatively higher values (Figure 2D). Overall, these observations suggest that while MM/GBSA can provide useful trends for hydrophobic binding sites, the stability and conformational behavior observed along MD trajectories offer a more reliable basis for assessing ligand-protein interactions and binding persistence.

TSA Confirmed Direct Binding of Several Compounds with Skp1

Direct binding between Skp1 and the 28 shortlisted compounds was confirmed using TSA. Both the intact ($Skp1^{WT}$) and truncated ($\Delta Skp1^{1-140}$) forms of recombinantly purified Skp1 were used for TSA. The previously reported Skp1 inhibitor, 6-OAP, was used as a positive control. Almost all the tested compounds were able to bind to $Skp1^{WT}$, with many inducing a temperature shift around or above the level of the positive control 6-OAP (Figure 4A). Interestingly, several compounds were also able to induce a marked temperature shift (ΔT_m around or above $3^{\circ}C$) for $\Delta Skp1^{1-140}$, albeit to a lesser extent than $Skp1^{WT}$ (Figure 4B), suggesting that their binding with the P1 region of Skp1 was consistent with our SBVS strategy. Compounds #20, #22, #24, #25, #27 and #28 were particularly interesting, for which the extent of temperature shift was similar in case of both $Skp1^{WT}$ and $\Delta Skp1^{1-140}$. Compound #24 induced an even more pronounced effect with $\Delta Skp1^{1-140}$. Notably, a few compounds (#04, #10, #17, and #21) failed to elicit a substantial temperature shift in $\Delta Skp1^{1-140}$, especially #04 showing no considerable stabilization. This observation suggests that the presence of the H8 helix (P2) is probably critical for the binding of these compounds. This notion is further corroborated by the substantially lower ΔT_m value ($2^{\circ}C$) for 6-OAP against $\Delta Skp1^{1-140}$ compared with $Skp1^{WT}$, which has previously been reported to interact with the H8-helix region.[12]

https://doi.org/10.2147/DDDT.S578211

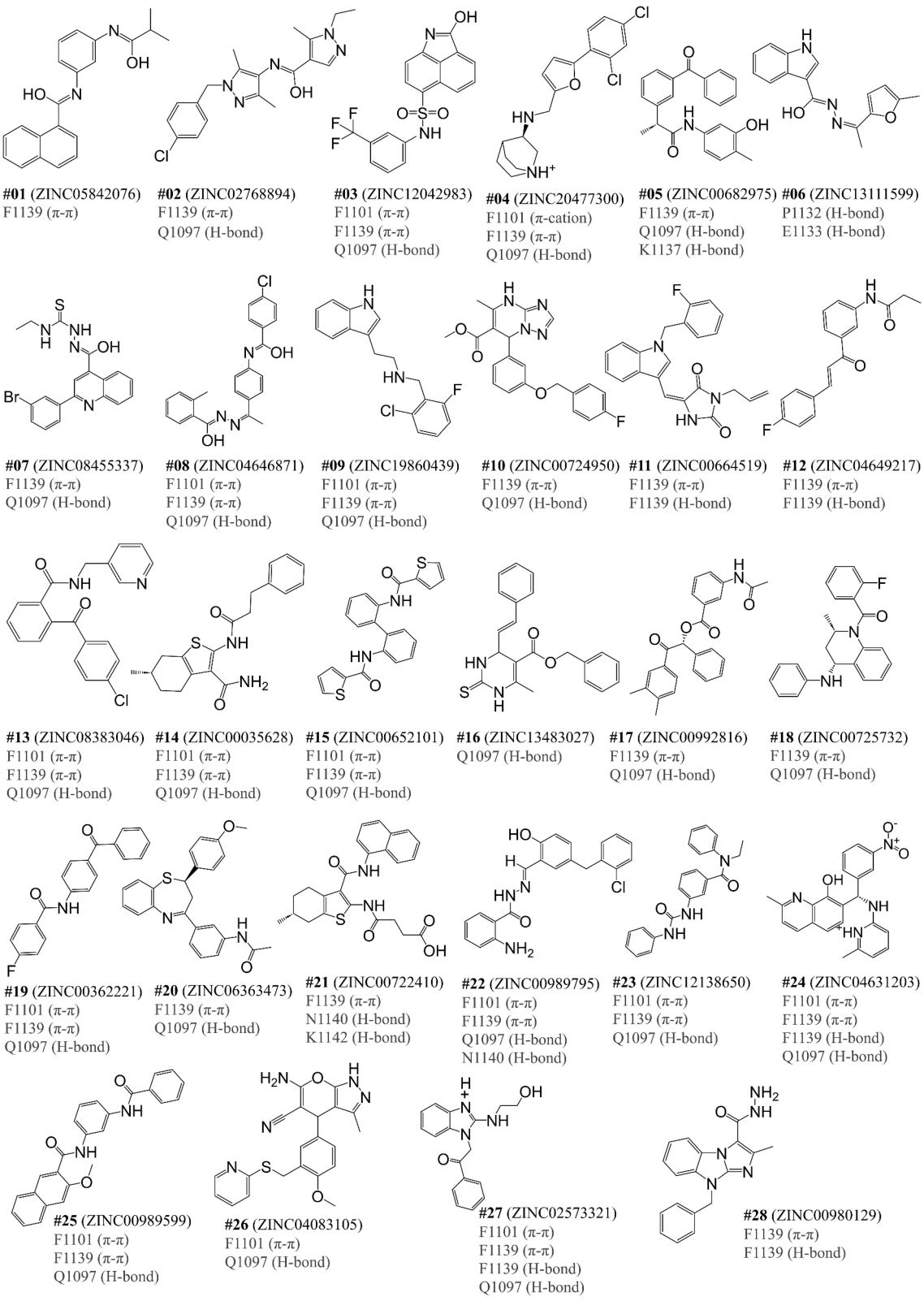

Figure 3 The chemical structures of the 28 shortlisted compounds and their interacting residues within the P1 hotspot of Skp1. # denotes the compound number.

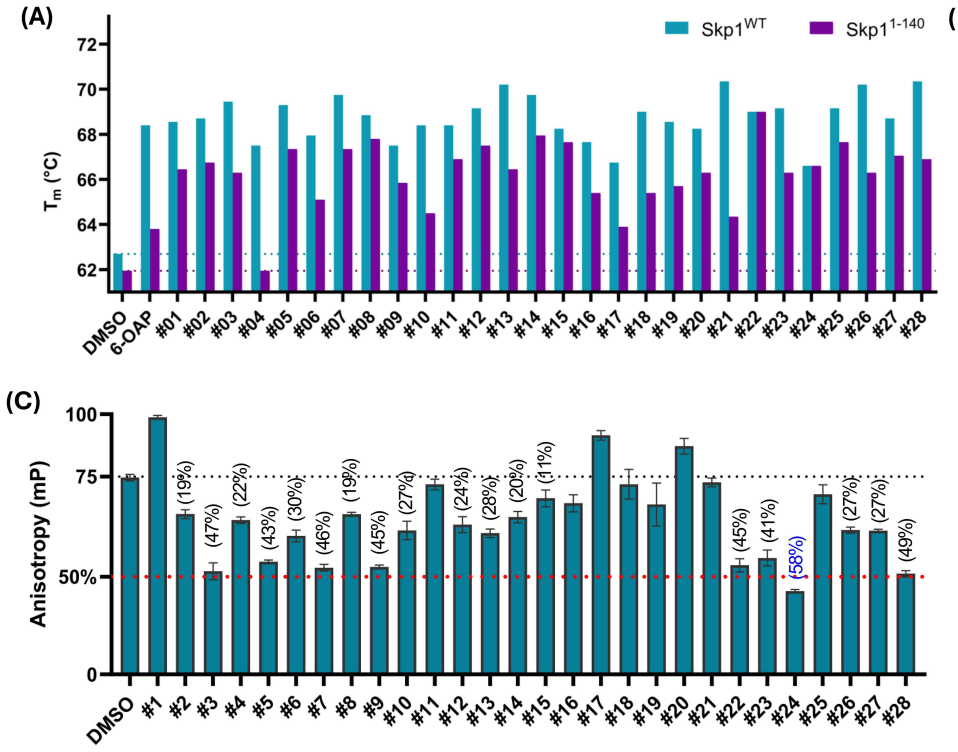

(B)

Compound	Skp1^{WT} ΔT_m (°C)	Skp1$^{1-140}$ ΔT_m (°C)
6-OAP	5.7	1.85
#01	5.85	4.5
#02	6	4.8
#03	6.75	4.35
#04	4.8	0
#05	6.6	5.4
#06	5.25	3.15
#07	7.05	5.4
#08	6.15	5.85
#09	4.8	3.9
#10	5.7	2.55
#11	5.7	4.95
#12	6.45	5.55
#13	7.5	4.5
#14	7.05	6
#15	5.55	5.7
#16	4.95	3.45
#17	4.05	1.95
#18	6.3	3.45
#19	5.85	3.75
#20	5.55	4.35
#21	7.65	2.4
#22	6.3	7.05
#23	6.45	4.35
#24	3.9	4.65
#25	6.45	5.7
#26	7.5	4.35
#27	6	5.1
#28	7.65	4.95

Figure 4 Biophysical and biochemical evaluation of shortlisted compounds by in vitro assays. (**A**) Average T_m (n = 2) for all compounds shortlisted in the screen calculated by TSA. Dotted horizontal lines indicate the DMSO baseline ΔT_m values for both Skp1^{WT} and Skp1$^{1-140}$. (**B**) ΔT_m calculated for each compound from the average T_m (n = 2). (**C**) Determination of Skp1:F-box peptide interaction inhibiting activity by FP assay. Data is represented as mean + SEM from triplicate experiments. The black dotted line indicates the upper anisotropy reference (100%) in the FP assay, while the red-dotted line represents the 50% inhibition threshold. The percentage inhibition of the prominent compound #24 is mentioned in blue.

Several Compounds Showed Inhibitory Activity Against Skp1:F-Box Interaction(s) in FP Assay

To verify that shortlisted compounds from SBVS could inhibit the Skp1:F-box interaction(s), we subjected them to FP-based Skp1-F-box in vitro biochemical assay.[21] Eight compounds (#03, #05, #07, #09, #22, #23, #24, and #28) inhibited the Skp1^{WT}:F-box interaction by ≥40% (Figure 4C). Especially, compound #24 caused more than 50% inhibition, while #03 and #28 showed inhibition almost at 50% borderline.

Cellular Level Evaluation of Anti-Tumor Activity

To facilitate the selection of hits for further optimization, we tested the growth inhibitory effects of SBVS shortlisted compounds in four adherent cancerous cell lines, including lung (A549), liver (HepG2), mammary (MCF7), and colon (HCT116) lines. The results indicated that these compounds exhibited varying degrees of inhibitory effects on the proliferation of the four cell lines. Compounds #04 and #12 potently inhibited the growth of all four cell lines, with EC_{50} values within the low-micromolar range of 3–9 μM (Table 1). Similarly, compound #24 also inhibited the growth of two cell lines (colon and liver) within the low-micromolar range and demonstrated moderately potent activity against the lung cancer line (16 μM). Compound #15 exhibited moderately potent activity against all four cell lines. In addition, compounds #22 and #28 displayed moderate activity against mammary and colon cancer lines, respectively. None of the other compounds demonstrated growth-inhibitory EC_{50} values less than 20 μM (data not shown). The 2D interaction maps of the viable selected hits are shown in Figure 5.

https://doi.org/10.2147/DDDT.S578211

Table 1 Evaluation of Growth Inhibitory Activity of Shortlisted Compounds in Different Cancer Cell Lines

No.	A549 (μM)	HepG2 (μM)	MCF7 (μM)	HCT116 (μM)
#04	8.88 ± 0.25	8.74 ± 0.16	9.10 ± 0.29	7.19 ± 0.04
#12	7.02 ± 0.43	4.54 ± 0.15	7.13 ± 0.16	3.73 ± 0.07
#15	19.35 ± 1.62	16.81 ± 0.92	14.76 ± 0.71	16.49 ± 0.71
#20	>20	19.6 ± 0.38	>20	16.28 ± 0.66
#22	>20	>20	8.36 ± 1.12	>20
#24	16.53 ± 2.23	9.82 ± 1.21	>20	4.42 ± 0.03
#28	>20	>20	>20	12.98 ± 0.46

Discussion

The efficacy of traditional SBVS approaches is generally limited for targeting the hydrophobic and structurally flexible PPI interfaces.[44] Unlike enzymes or receptors with well-defined binding pockets, PPIs typically present shallow, dynamic, and poorly delineated hotspots, which undergo conformational rearrangements upon ligand or partner engagement. Consequently, these features pose significant challenges for rigid docking and conventional scoring

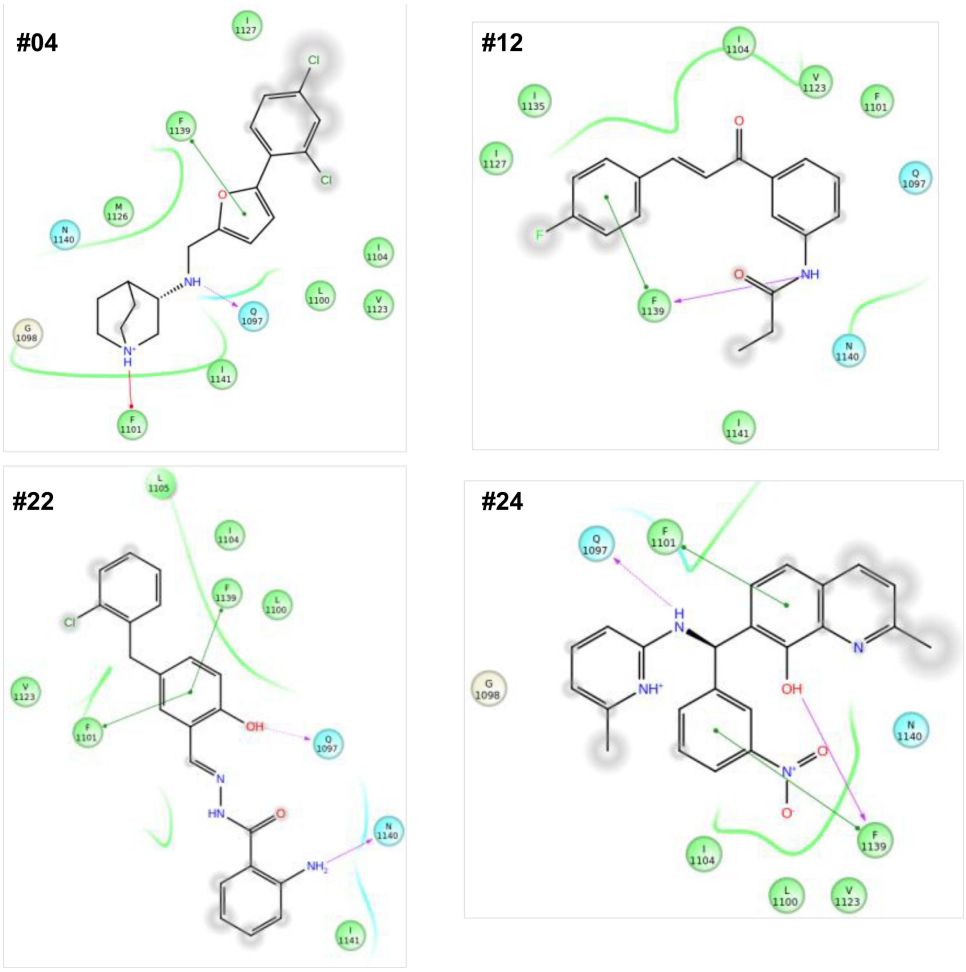

Figure 5 2D interaction plots of selected hits against Skp1. Purple arrow indicates H-bond interaction, while the green dotted line represents π-π or π-cation interactions.

functions.[42,44,45] However, incorporating protein dynamics, MD simulations, or induced-fit modeling, followed by rescoring using physics-based free energy methods (eg. MM/GBSA or MM/PBSA), can substantially improve prediction accuracy by capturing conformational adaptation and nonpolar solvation effects.[42,43] One may anticipate that binding is inherently dynamic rather than a static event; therefore, understanding (exploring) the conformational flexibility of the target protein is critical. In this context, ligand-protein MD simulations in the 60–100 ns range are commonly used as a pragmatic compromise between computational cost and the need to observe whether a ligand remains stably bound and maintains key binding interactions under dynamic conditions.[46,47]

The MD-integrated SBVS workflow employed in this study provides a rational strategy for identifying potential Skp1:F-box PPI inhibitors, ensuring both the physicochemical suitability and structural relevance of the screened compounds. This multi-tiered approach minimizes false positives typically associated with high-throughput docking and enhances the likelihood of discovering tractable chemical scaffolds for optimization. Notably, ΔMM/GBSA, particularly suited for the hydrophobic nature of the P1 hotspot, provides reliable insights into the thermodynamic determinants governing ligand–protein interactions. Although several compounds exhibited moderate positional fluctuations during MD trajectories, their binding was largely maintained throughout the simulations. This observation reinforces the importance of integrating MD simulations with careful trajectory analysis to assess the stability and plausibility of ligand–protein interactions beyond numerical scoring.

In the subsequent biophysical evaluation, nearly all compounds induced measurable thermal stabilization of Skp1 in the TSA ($\Delta T_m > 3°C$),[48] indicating specific target engagement. Several compounds showed binding to both the intact and truncated (containing only the P1 hotspot) forms of Skp1, consistent with our SBVS strategy centered on this region. Nonetheless, compounds #04, #10, #17, and #21 exhibited a distinct dependence on the adjacent H8 helix. The loss of thermal stabilization upon truncation ($\Delta Skp1^{1–140}$) for these compounds suggests that the H8 helix probably contributes critical binding contacts, likely through transient interactions at the F-box interface. These findings underscore the importance of considering the local structural dynamics in large-scale SBVS campaigns targeting flexible PPI surfaces.

In the biochemical FP assay, eight compounds (#03, #05, #07, #09, #22, #23, #24, and #28) inhibited the Skp1:F-box peptide interaction by >40% (Figure 4C), consistent with typical hit selection criteria for FP-based PPI screens.[49] In particular, compounds #03, #22, #24, and #28 showed inhibition near or below the 50% value. Furthermore, in the cell viability assay, compounds #04, #12, and #24 demonstrated EC_{50} values in the low-micromolar range. Notably, compound #24, featuring a quinoline-based structural core analogous to the previously reported Skp1 inhibitor Z0933M, has emerged as an interesting scaffold for future structure-activity relationship studies. The observation that compound #07 contains a quinoline-4-carbohydrazonic acid moiety and causes >40% inhibition further supports the notion that quinoline scaffolds may represent as a privileged chemotype for engaging the F-box binding interface of Skp1. Apart from this, compounds #04 and #12 also warrant particular attention. Notably, compound #04 lost the T_m shift signal with the truncated Skp1 variant ($Skp1^{1–140}$), whereas compound #12 retained a reasonable T_m shift signal with this construct. Despite this different behaviour in TSA assay, both compounds demonstrated low-micromolar antiproliferative activity in the cell viability assay (Table 1). Furthermore, although neither compound surpassed the ≥40% inhibition threshold in the FP assay, both exhibited measurable albeit weaker disruption of the Skp1:F-box interaction relative to other biochemically active compounds (Figure 4C). Together, these observations suggest that compounds #04 and #12 may represent distinct chemotypes capable of modulating Skp1 function through mechanisms that are not fully captured by a single biochemical assay format. Their cellular activity, combined with detectable biochemical engagement, presents them attractive candidates for further mechanistic investigation and optimization.

Specifically emphasizing compound #04, the current TSA data indicate that its binding mode may involve structural elements outside the minimal P1 hotspot retained in $Skp1^{1–140}$. This remains plausible with the initial docking steps. The Glide grid, while centered on the P1 region, may have permitted partial engagement of adjacent interface region, including elements of the P2/H8 region due to the relatively shallow and spatially extended nature of the Skp1 F-box interface. Moreover, given the dynamic nature of the PPI surface, it is also possible that compound #04 engages a conformationally stabilized interface that is not fully recapitulated in the truncated construct. In brief, such context-dependent binding could explain the reduced thermal stabilization observed with $Skp1^{1–140}$. Notably, certain degree of reduction in T_m shift signal of several other compounds was also observed when tested with $Skp1^{1–140}$ (Figure 4A and

 https://doi.org/10.2147/DDDT.S578211

B), further corroborating the notion that contributions from regions beyond the minimal P1 hotspot may be required for optimal stabilization.

Several other molecules identified in this study which caused >40% inhibition of Skp1:F-box peptide interaction—such as #03 (2-hydroxy-N-(3-(trifluoromethyl)phenyl)benzo[cd]indole-6-sulfonamide), #05 ((R)-2-(3-benzoylphenyl)-N-(3-hydroxy-4-methylphenyl)propanamide), #09 (N-(2-chloro-6-fluorobenzyl)-2-(1H-indol-3-yl)ethan-1-amine), #22 ((E)-2-amino-N′-(5-(2-chlorobenzyl)-2-hydroxybenzylidene)benzohydrazide), and #28 (9-benzyl-2-methyl-9H-benzo[d]imidazo[1,2-a]imidazole-3-carbohydrazide)—share structural features commonly reported as useful traits of PPI inhibitors.[26,45,50–53] These include extended hydrophobic aromatic systems that can complement the nonpolar nature of shallow binding surfaces, as well as hydrogen-bond donor–acceptor networks and halogenated substituents that may stabilize transient binding through directional interactions. The coexistence of these physicochemical features is often associated with the ability of small molecules to interact with PPI hotspots and shallow binding interfaces.[44,50,51,54,55] Binding pose analyses of all these compounds further indicated that they formed aromatic stacking and hydrogen bonding interactions with the hotspot residues, such as F1101, F1139, and Q1097 (Figure S2 and Figure 3). Together, these observations suggest that the identified scaffolds may exploit transient or hydrophobic hotspots at the Skp1 interface. While several of these compounds did not exhibit measurable anti-proliferative effects, their ability to disrupt Skp1:F-box PPIs in vitro highlights their potential as starting points for medicinal chemistry refinement, a common limitation of early-stage PPI inhibitors.[44,53,56] Subsequent optimization may focus on improving the cell permeability and intracellular target engagement.

Small molecules engaging hydrophobic PPI hotspots may sometimes exhibit promiscuous binding or non-specific effects as they frequently rely on lipophilicity-driven interactions to achieve sufficient surface complementarity.[44,57] Given that the identified hits target a hydrophobic hotspot region within the Skp1 F-box interface, potential selectivity and off-target considerations warrant careful evaluation. In this context, the observed reduction in cell viability should be interpreted carefully at this early stage. Although our biophysical (TSA) and biochemical (FP) assays support direct Skp1 binding and functional disruption of the interaction in vitro, the observed cellular responses may not exclusively reflect on-target Skp1 inhibition in cellulo. Instead, they could arise, at least in part, from broader pathway perturbations or off-target mechanisms commonly associated with hydrophobic PPI modulators.[57,58] Finally, although the initial 28 hits were prioritized based on predicted favorable ADMET parameters, only compounds #04, #12, #15, and #24 demonstrated measurable cellular activity. This attrition is not unexpected, particularly in the context of PPI inhibitors. While computational ADMET filtering enriches for drug-like candidates, it generally does not account for intracellular target engagement, residence time, or context-dependent protein complex formation, factors typically relevant for PPI targets.[56] Therefore, further orthogonal validation incorporating strategies like cellular target engagement assays, genetic rescue approaches, and selectivity assessments will be important to establish a clear mechanistic link to Skp1 inhibition.

Conclusion

Given that Skp1 overexpression or hyperactivation contributes to tumor initiation and progression, therapeutic targeting of Skp1 may be a promising treatment option for tumors. Building on our previous work,[2,12,21] this study employed an MD-integrated SBVS approach to identify new chemical scaffolds that engage the P1 hotspot at the F-box binding interface. The identified compounds can be viewed as attractive starting points for medicinal chemistry optimization toward potent Skp1:F-box PPI inhibitors. We anticipate that future chemical optimization of compounds #04, #12, #15, and #24 may give rise to next-generation Skp1 inhibitors.

Acknowledgments

MH and MT were previously sponsored by the CAS-TWAS President's Fellowship for International PhD Students. MH is also thankful to the China Postdoctoral Science Foundation and the Guangdong Provincial Postdoctoral Special Funding. The authors gratefully acknowledge support from the Guangzhou Branch of the Supercomputing Center of the Chinese Academy of Sciences.

Author Contributions

All authors made a significant contribution to the work reported, whether that is in the conception, study design, execution, acquisition of data, analysis and interpretation, or in all these areas; took part in drafting, revising or critically reviewing the article; gave final approval of the version to be published; have agreed on the journal to which the article has been submitted; and agree to be accountable for all aspects of the work.

Disclosure

The authors declare that they have no known competing interests in this work.

References

1. Bai C, Sen P, Hofmann K, et al. SKP1 connects cell cycle regulators to the ubiquitin proteolysis machinery through a novel motif, the F-box. *Cell*. 1996;86(2):263–274. doi:10.1016/s0092-8674(00)80098-7
2. Hussain M, Lu Y, Liu YQ, et al. Skp1: implications in cancer and SCF-oriented anti-cancer drug discovery. *Pharmacol Res*. 2016;111:34–42. doi:10.1016/j.phrs.2016.05.027
3. Zhou YH, Xia J, Xu WH, et al. Cullin-1 promotes cell proliferation in human breast cancer and is related to diabetes. *Int J Biol Markers*. 2016;31 (4):e375–e381. doi:10.5301/jbm.5000215
4. Jiang H, He D, Xu H, Liu J, Qu L, Tong S. Cullin-1 promotes cell proliferation via cell cycle regulation and is a novel in prostate cancer. *Int J Clin Exp Pathol*. 2015;8(2):1575–1583.
5. Shao J, Feng Q, Jiang W, et al. E3 ubiquitin ligase RBX1 drives the metastasis of triple negative breast cancer through a FBXO45-TWIST1-dependent degradation mechanism. *Aging*. 2022;14(13):5493–5510. doi:10.18632/aging.204163
6. Migita K, Takayama T, Matsumoto S, et al. Prognostic impact of RING box protein-1 (RBX1) expression in gastric cancer. *Gastric Cancer*. 2014;17(4):601–609. doi:10.1007/s10120-013-0318-y
7. Cheng J, Liu O, Bin X, Tang Z. F-box proteins in cancer: from cancer cells to the tumor microenvironment. *Cell Commun Signal*. 2025;23(1):433. doi:10.1186/s12964-025-02445-z
8. Yumimoto K, Yamauchi Y, Nakayama KI. F-Box proteins and cancer. *Cancers*. 2020;12(5):1249. doi:10.3390/cancers12051249
9. Lepage CC, Palmer MCL, Farrell AC, et al. Reduced SKP1 and CUL1 expression underlies increases in Cyclin E1 and chromosome instability in cellular precursors of high-grade serous ovarian cancer. *Br J Cancer*. 2021;124(10):1699–1710. doi:10.1038/s41416-021-01317-w
10. Thompson LL, Baergen AK, Lichtensztejn Z, McManus KJ. Reduced SKP1 expression induces chromosome instability through aberrant cyclin E1 protein turnover. *Cancers*. 2020;12(3):531. doi:10.3390/cancers12030531
11. Tian C, Lang T, Qiu J, et al. SKP1 promotes YAP-mediated colorectal cancer stemness via suppressing RASSF1. *Cancer Cell Int*. 2020;20(1):579. doi:10.1186/s12935-020-01683-0
12. Liu YQ, Wang XL, Cheng X, et al. Skp1 in lung cancer: clinical significance and therapeutic efficacy of its small molecule inhibitors. *Oncotarget*. 2015;6(33):34953–34967. doi:10.18632/oncotarget.5547
13. Shiba-Ishii A, Hong J, Hirokawa T, et al. Stratifin inhibits SCF(FBW7) formation and blocks ubiquitination of oncoproteins during the course of lung adenocarcinogenesis. *Clin Cancer Res*. 2019;25(9):2809–2820. doi:10.1158/1078-0432.CCR-18-3631
14. Quan J, Ma C. DNMT1-mediated regulating on FBXO32 promotes the progression of glioma cells through the regulation of SKP1 activity. *Environ Toxicol*. 2023;39:783–793. doi:10.1002/tox.23976
15. Wu S, Yang J, Xu H, et al. Circular RNA circGLIS3 promotes bladder cancer proliferation via the miR-1273f/SKP1/Cyclin D1 axis. *Cell Biol Toxicol*. 2022;38(1):129–146. doi:10.1007/s10565-021-09591-3
16. Zhu H, Zhang H, Pei Y, et al. Long non-coding RNA CCDC183-AS1 acts AS a miR-589-5p sponge to promote the progression of hepatocellular carcinoma through regulating SKP1 expression. *J Exp Clin Cancer Res*. 2021;40(1):57. doi:10.1186/s13046-021-01861-6
17. Zeng J, Chen Z, He Y, et al. A patent review of SCF E3 ligases inhibitors for cancer:Structural design, pharmacological activities and structure-activity relationship. *Eur J Med Chem*. 2024;278:116821. doi:10.1016/j.ejmech.2024.116821
18. Liu J, Peng Y, Zhang J, Long J, Liu J, Wei W. Targeting SCF E3 Ligases for Cancer Therapies. *Adv Exp Med Biol*. 2020;1217:123–146. doi:10.1007/978-981-15-1025-0_9
19. Kitagawa K, Kitagawa M. The SCF-type E3 Ubiquitin Ligases as Cancer Targets. *Curr Cancer Drug Targets*. 2016;16(2):119–129. doi:10.2174/1568009616666151112122231
20. Soucy TA, Smith PG, Milhollen MA, et al. An inhibitor of NEDD8-activating enzyme as a new approach to treat cancer. *Nature*. 2009;458 (7239):732–736. doi:10.1038/nature07884
21. Hussain M, Lu Y, Tariq M, et al. A small-molecule Skp1 inhibitor elicits cell death by p53-dependent mechanism. *iScience*. 2022;25(7):104591. doi:10.1016/j.isci.2022.104591
22. Chan CH, Morrow JK, Li CF, et al. Pharmacological inactivation of Skp2 SCF ubiquitin ligase restricts cancer stem cell traits and cancer progression. *Cell*. 2013;154(3):556–568. doi:10.1016/j.cell.2013.06.048
23. Huang KS, Vassilev LT. High-throughput screening for inhibitors of the Cks1-Skp2 interaction. *Methods Enzymol*. 2005;399:717–728. doi:10.1016/S0076-6879(05)99047-2
24. Wu L, Grigoryan AV, Li Y, Hao B, Pagano M, Cardozo TJ. Specific small molecule inhibitors of Skp2-mediated p27 degradation. *Chem Biol*. 2012;19(12):1515–1524. doi:10.1016/j.chembiol.2012.09.015
25. Xing S, Nong F, Wang Y, et al. Brusatol has therapeutic efficacy in non-small cell lung cancer by targeting Skp1 to inhibit cancer growth and metastasis. *Pharmacol Res*. 2022;176:106059. doi:10.1016/j.phrs.2022.106059
26. Li X, Mamouni K, Zhao R, et al. Novel Skp1 inhibitor has potent preclinical efficacy against castration-resistant prostate cancer. *Br J Cancer*. 2025;132(12):1188–1199. doi:10.1038/s41416-025-02993-8

27. Bulatov E, Ciulli A. Targeting Cullin-RING E3 ubiquitin ligases for drug discovery: structure, assembly and small-molecule modulation. *Biochem J*. 2015;467(3):365–386. doi:10.1042/BJ20141450
28. Cai SJ, Liu Y, Han S, Yang C. Brusatol, an NRF2 inhibitor for future cancer therapeutic. *Cell Biosci*. 2019;9:45. doi:10.1186/s13578-019-0309-8
29. Hwang N, Pei Y, Clement J, Robertson ES, Du Y. Identification of a 3-beta-homoalanine conjugate of brusatol with reduced toxicity in mice. *Bioorg Med Chem Lett*. 2020;30(23):127553. doi:10.1016/j.bmcl.2020.127553
30. Cheng X, Liu YQ, Wang GZ, et al. Proteomic identification of the oncoprotein STAT3 as a target of a novel Skp1 inhibitor. *Oncotarget*. 2017;8 (2):2681–2693. doi:10.18632/oncotarget.13153
31. Makafe GG, Hussain M, Surineni G, et al. Quinoline derivatives kill Mycobacterium tuberculosis by activating glutamate kinase. *Cell Chem Biol*. 2019;26(8):1187–1194e5. doi:10.1016/j.chembiol.2019.05.003
32. Trott O, Olson AJ. AutoDock Vina: improving the speed and accuracy of docking with a new scoring function, efficient optimization, and multithreading. *J Comput Chem*. 2010;31(2):455–461. doi:10.1002/jcc.21334
33. Sanner MF. Python: a programming language for software integration and development. *J Mol Graph Model*. 1999;17(1):57–61.
34. Wan-Mamat WM, Isa NA, Wahab HA, Wan-Mamat WM. Drug-like and non drug-like pattern classification based on simple topology descriptor using hybrid neural network. *Ann Int Conf IEEE Eng Med Biol Soc*. 2009; 2009:6424–6427. doi:10.1109/IEMBS.2009.5333747
35. Zhou Y, Hussain M, Kuang G, Zhang J, Tu Y. Mechanistic insights into peptide and ligand binding of the ATAD2-bromodomain via atomistic simulations disclosing a role of induced fit and conformational selection. *Phys Chem Chem Phys*. 2018;20(36):23222–23232. doi:10.1039/c8cp03860k
36. Wang J, Wolf RM, Caldwell JW, Kollman PA, Case DA. Development and testing of a general amber force field. *J Comput Chem*. 2004;25 (9):1157–1174. doi:10.1002/jcc.20035
37. Price DJ, Brooks CL. A modified TIP3P water potential for simulation with Ewald summation. *J Chem Phys*. 2004;121(20):10096–10103. doi:10.1063/1.1808117
38. Ruymgaart AP, Elber R. Revisiting molecular dynamics on a CPU/GPU system: water kernel and SHAKE parallelization. *J Chem Theory Comput*. 2012;8(11):4624–4636. doi:10.1021/ct300324k
39. Osguthorpe DJ, Sherman W, Hagler AT. Generation of receptor structural ensembles for virtual screening using binding site shape analysis and clustering. *Chem Biol Drug Des*. 2012;80(2):182–193. doi:10.1111/j.1747-0285.2012.01396.x
40. Bottegoni G, Rocchia W, Rueda M, Abagyan R, Cavalli A. Systematic exploitation of multiple receptor conformations for virtual ligand screening. *PLoS One*. 2011;6(5):e18845. doi:10.1371/journal.pone.0018845
41. Chandra Dantu S, Nathubhai Kachariya N, Kumar A. Molecular dynamics simulations elucidate the mode of protein recognition by Skp1 and the F-box domain in the SCF complex. *Proteins*. 2016;84(1):159–171. doi:10.1002/prot.24963
42. Zhang X, Perez-Sanchez H, Lightstone FC. A comprehensive docking and MM/GBSA rescoring study of ligand recognition upon binding antithrombin. *Curr Top Med Chem*. 2017;17(14):1631–1639. doi:10.2174/1568026616666161117112604
43. Wang E, Sun H, Wang J, et al. End-point binding free energy calculation with MM/PBSA and MM/GBSA: strategies and applications in drug design. *Chem Rev*. 2019;119(16):9478–9508. doi:10.1021/acs.chemrev.9b00055
44. Nada H, Choi Y, Kim S, Jeong KS, Meanwell NA, Lee K. New insights into protein-protein interaction modulators in drug discovery and therapeutic advance. *Signal Transduct Target Ther*. 2024;9(1):341. doi:10.1038/s41392-024-02036-3
45. Guo W, Wisniewski JA, Ji H. Hot spot-based design of small-molecule inhibitors for protein-protein interactions. *Bioorg Med Chem Lett*. 2014;24 (11):2546–2554. doi:10.1016/j.bmcl.2014.03.095
46. Pirolli D, Righino B, Camponeschi C, Ria F, Di Sante G, De Rosa MC. Virtual screening and molecular dynamics simulations provide insight into repurposing drugs against SARS-CoV-2 variants Spike protein/ACE2 interface. *Sci Rep*. 2023;13(1):1494. doi:10.1038/s41598-023-28716-8
47. Macalino SJY, Basith S, Clavio NAB, Chang H, Kang S, Choi S. Evolution of in silico strategies for protein-protein interaction drug discovery. *Molecules*. 2018;23(8). doi:10.3390/molecules23081963
48. Coyle J, Walser R. Applied biophysical methods in fragment-based drug discovery. *SLAS Discov*. 2020;25(5):471–490. doi:10.1177/2472555220916168
49. Fancher AT, Hua Y, Camarco DP, Close DA, Strock CJ, Johnston PA. High-content screening campaign to identify compounds that inhibit or disrupt androgen receptor-transcriptional intermediary factor 2 protein-protein interactions for the treatment of prostate cancer. *Assay Drug Dev Technol*. 2018;16(6):297–319. doi:10.1089/adt.2018.858
50. Wu D, Li Y, Zheng L, et al. Small molecules targeting protein-protein interactions for cancer therapy. *Acta Pharm Sin B*. 2023;13(10):4060–4088. doi:10.1016/j.apsb.2023.05.035
51. Smith MC, Gestwicki JE. Features of protein-protein interactions that translate into potent inhibitors: topology, surface area and affinity. *Expert Rev Mol Med*. 2012;14:e16. doi:10.1017/erm.2012.10
52. Aeluri M, Chamakuri S, Dasari B, et al. Small molecule modulators of protein-protein interactions: selected case studies. *Chem Rev*. 2014;114 (9):4640–4694. doi:10.1021/cr4004049
53. Arkin MR, Tang Y, Wells JA. Small-molecule inhibitors of protein-protein interactions: progressing toward the reality. *Chem Biol*. 2014;21 (9):1102–1114. doi:10.1016/j.chembiol.2014.09.001
54. Demirel HC, Dogan T, Tuncbag N. A structural perspective on the modulation of protein-protein interactions with small molecules. *Curr Top Med Chem*. 2018;18(8):700–713. doi:10.2174/1568026618666180601080824
55. Rognan D. Rational design of protein–protein interaction inhibitors. *MedChemComm*. 2015;6:51–60. doi:10.1039/c4md00328d
56. Lagorce D, Douguet D, Miteva MA, Villoutreix BO. Computational analysis of calculated physicochemical and ADMET properties of protein-protein interaction inhibitors. *Sci Rep*. 2017;7:46277. doi:10.1038/srep46277
57. Lu H, Zhou Q, He J, et al. Recent advances in the development of protein-protein interactions modulators: mechanisms and clinical trials. *Signal Transduct Target Ther*. 2020;5(1):213. doi:10.1038/s41392-020-00315-3
58. Thangudu RR, Bryant SH, Panchenko AR, Madej T. Modulating protein-protein interactions with small molecules: the importance of binding hotspots. *J Mol Biol*. 2012;415(2):443–453. doi:10.1016/j.jmb.2011.12.026